Microscopic structure and collapse of depletion-induced gels in vesicle-polymer mixtures

Ji Yeon Huh,[1] Matthew L. Lynch,[2,*] and Eric M. Furst[1,†]
[1]*Department of Chemical Engineering, University of Delaware, Colburn Laboratory, 150 Academy Street, Newark, Delaware 19716, USA*
[2]*Corporate Research Division, Procter and Gamble Company, Miami Valley Laboratory, 11810 East Miami Road, Cincinnati, Ohio 45252-1038, USA*
(Received 19 July 2007; published 29 November 2007)

We present the behavior of depletion-induced gels for vesicle-polymer mixtures when the ratio of the polymer radius of gyration to the mean vesicle radius is 0.09 and 0.27. As the polymer concentration increases, density gradients build up and an interface is developed between a highly turbid vesicle-rich phase and a polymer-rich phase. Increasing the polymer concentration further forms a gel (C_P=0.3 and 0.1 wt % for $R_g/a \approx 0.09$ and 0.27, respectively), which subsequently collapses. This collapse is characterized by a slow initial rising for a finite delay time, a rapid collapse, and a slow final compaction to an equilibrium height. However, we observe a remarkably different polymer concentration dependence on the collapse rate. Unlike other colloidal gels, we find that the delay time for the vesicle collapse decreases with increasing polymer concentration. We show that this behavior can be accounted for by considering the permeability for solvent backflow, which is directly related to the characteristic pore area of the gel obtained using confocal microscopy.

DOI: 10.1103/PhysRevE.76.051409 PACS number(s): 82.70.Dd, 82.70.Gg, 82.70.Uv

I. INTRODUCTION

In the presence of weak attractive interactions, colloidal particles aggregate, forming space spanning networks that are transient and nonequilibrium in nature [1,2]. When the density of the colloidal particles differs from that of the suspending medium, a transient gel is a consequence of both Brownian motion and the imposed gravitational field. This eventually leads to the collapse of the gel. For strong interparticle attractions ($U \geqslant 10k_BT$), the collapse occurs smoothly. As the attractive interaction is reduced, the gel is initially stable for some finite time before it rapidly collapses, which is known as a delayed sedimentation [1,3–7]. Since gel collapse is typically an undesirable phenomenon that affects the stability and shelf life of many food and personal care products, understanding and controlling this issue remains a crucial aim.

In this paper, we report the study of the microstructure and collapse of gels in vesicle-polymer mixtures. Weak and moderately strong attractive interactions between the vesicles are induced by depletion forces caused by the nonadsorbing polymer. Studies of such vesicle-polymer mixtures are of particular interest because they are useful for many applications, including foods, cosmetics, plastics, pesticides, and paints [8]. Vesicle dispersions are further critical for emerging applications, such medical imaging and gene therapies [9,10]. Unlike other colloidal particles, vesicles lead to additional and interesting complexity because they are polydisperse, soft, and often nonspherical [11].

Following the details of our experimental approach, we present the phase behavior of vesicle-polymer mixtures identified as phase separation and collapse of depletion gels. From the time evolution in the height, we discuss the collapse rate and delay time, which is a strong function of the polymer concentration. We correlate the permeability derived from the theory of the initial sedimentation velocity to the characteristic pore area obtained from confocal microscopy. Finally, we conclude with the implications and future directions of this work.

II. EXPERIMENT

The vesicle dispersion is prepared from an aqueous solution of the dichain cationic surfactant, ditallowethylester dimethyl ammonium chloride (Goldsmith), with standard milling manufacturing process. They are quaternary ammonium compounds which have two long fatty acid chains with two weak ester linkages. The vesicles have a mean diameter of 256±23 nm, as measured by dynamic light scattering (DLS). The correlation functions are analyzed using CONTIN algorithms (Brookhaven BI-200SM goniometer at 90°, BI-9000AT autocorrelation card, and Coherent INNOVA 300 argon ion laser operating at λ=514.5 nm). There are a couple of notes regarding the apparent contradiction with the DLS measurements and microscopy images. DLS measurements provide the average, weighted by particle diameter and relative volume fraction. These values have been used to quantify average interparticle interactions and sedimentation theory. We note that the phase behavior agrees well with Asakura-Oosawa theory using such averaged quantities, validating this approximation. In contrast, microscopy captures the entire range of sizes and perhaps is visually weighted more towards the rarest, largest particle sizes. The volume fraction of the dispersion is determined to be ϕ=0.46 by separating a vesicle layer with centrifugation using 40 000 rpm for 18 h at 25 °C and adjusting it by a factor of 0.7, the packing efficiency of polydisperse spheres. Figure 1

*Corresponding author. FAX: (513) 627-1233. lynch.ml@pg.com
†Corresponding author. FAX: (302) 831-1048. furst@udel.edu

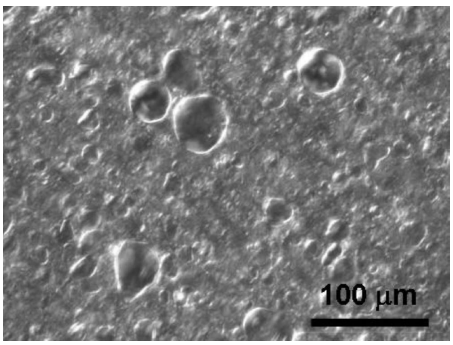

FIG. 1. Bright-field image of the vesicle dispersions at $\phi=0.46$ (DIC 40 × objective) showing the polydispersed distribution of the vesicle size.

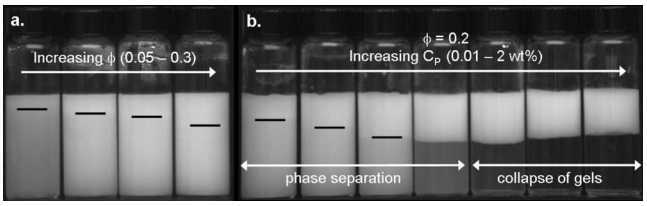

FIG. 2. Images obtained 30 days after samples are prepared. (a) The control samples in the absence of polymer, from left to right, $\phi=0.05,0.15,0.2,0.3$. The solid line is shown to emphasize very subtle phase separation. (b) From left to right, $C_P=0.01,0.05,0.1,0.2,0.3,1.2,2.0$ wt % at $\phi=0.2$ and $R_g/a\approx0.09$. The vesicles form a network and collapse above $C_P=0.3$ wt %, which is clearly distinguished from classical phase separation by the clear supernatant.

is a bright-field image of the vesicle dispersion that shows the polydisperse distribution of vesicle sizes.

The polymer used in this study is poly(diallyldimethylammoniumchloride) (polyDADMAC, Aldrich, No. 522376), which is cationic. The high charge prevents significant adsorption of the polymer on the vesicles. It is highly water soluble and available in various molecular weights (MWs). We use polyDADMAC with MW=14500 g/mol ($R_g=11.2$ nm and $R_g/a\approx0.09$) and 410000 g/mol ($R_g=35.3$ nm and $R_g/a\approx0.27$) determined by DLS and gel permeation chromatography (GPC). The GPC measurements show the polydispersity index (PDI) as 3.1 and 4.1 for 14.5 kDa and 410 kDa, respectively.

The formation of microstructure of vesicles dispersed in polyDADMAC is captured using the Nikon E400POL fluorescence microscopy with a 20-W mercury lamp and a Texas Red HYQ filter. The samples are mixed with a small amount of Nile Red dye (Aldrich, No. N3013) dissolved in dimethylform (DMF). To visualize the microstructure directly, confocal microscopy is also used (Nipkow confocal, Yokogawa Electric Co. Model CSU 10). Images are captured using a 10-bit-intensified charge-coupled device (CCD) camera (Stanford Photonics XR-MEGA/10).

Viscoelastic properties of the vesicle dispersions are measured using both bulk and microrheology. Frequency sweep rheology experiments are performed at constant stress $\sigma_0=0.01$ Pa from 0.1 to 10 Hz in a Couette geometry (AR 2000, TA Instruments). All the samples are measured immediately after mixing at 25 °C. The storage (G') and loss moduli (G'') and the complex viscosity (η^*) are determined as a function of time scale. Diffusing wave spectroscopy (DWS) is used to quantify the evolution of vesicle mobility on the order of $10^{-6}-1$ s to characterize the viscoelastic properties without perturbing a weak gel network. DWS experiments are made in a transmission geometry with an argon ion laser (Coherent INNOVA 300, wavelength $\lambda=514.5$ nm). Scattered light is collected with a collimated single-mode fiber optic which splits the signal 50/50. The split signal is collected with matched photon multiplier tubes (Brookhaven Instruments), and the intensity autocorrelation of the scattered light $\langle I(0)I(t)\rangle/\langle I\rangle^2$ is calculated using a cross-correlation mode over delay times between 25 ns and 500 ms with a BI-9000AT correlator (Brookhaven Instruments). The field autocorrelation function $g^{(1)}(t)$ is obtained via the Siegert relation $\langle I(0)I(t)\rangle/\langle I\rangle^2=1+\beta|g_1(t)^2|$ where the intercept β accounts for the optical properties of our apparatus. The mean-squared displacement (MSD) of vesicles is numerically calculated from the field autocorrelation function for the transmission geometry [12]. The width of cell is $l=6$ mm. The photon mean free path l^*, the length over which the scattered light is completely randomized, is measured by comparing the average transmitted light intensity against a 450-nm polystyrene bead standard (Duke Scientific, No. N3450A). We find $l^*=0.86-0.55$ mm for vesicle volume fraction $\phi=0.05-0.3$.

III. RESULTS AND DISCUSSION

A. Delayed rising

To begin, the phase behavior of vesicle-polymer mixtures is investigated as a function of both vesicle and polymer concentrations. Vesicle dispersions with volume fractions $\phi=0.05-0.3$ are systematically mixed with polymer concentrations ranging from 0.01 to 2.0 wt %. All samples are prepared in a cylindrical cell of diameter of 2 cm, and the initial sample height h_0 is kept as 4 cm. We mix the samples at high speeds prior to each measurement, ensuring that they are well dispersed. The density difference between the vesicle and the solvent is $\Delta\rho\approx50$ kg/m^3. In the absence of polymer, the vesicle dispersions remain stable or show subtle separation due to the density difference indicated by a solid line in Fig. 2(a). Separation is observed after long times and is distinguishable from vesicle-polymer mixtures, which phase separate immediately after the addition of polymer due to the depletion interaction. In the presence of polymer, density gradients build up and the dispersions separate into a highly turbid vesicle-rich phase on top and a polymer-rich phase on the bottom up to $C_P=0.2$ and 0.05 wt % for $R_g/a\approx0.09$ and 0.27, respectively. Increasing the polymer concentration further results in a collapsing vesicle-gel network. As compared in Fig. 2(b), this is clearly distinguished from classical phase separation where the bottom is turbid, indicating the presence of a dilute vesicle fluid by visual inspection. Empirically, the gel line appears consistently for all volume fractions at $C_P=0.3$ and 0.1 wt % for $R_g/a\approx0.09$ and 0.27,

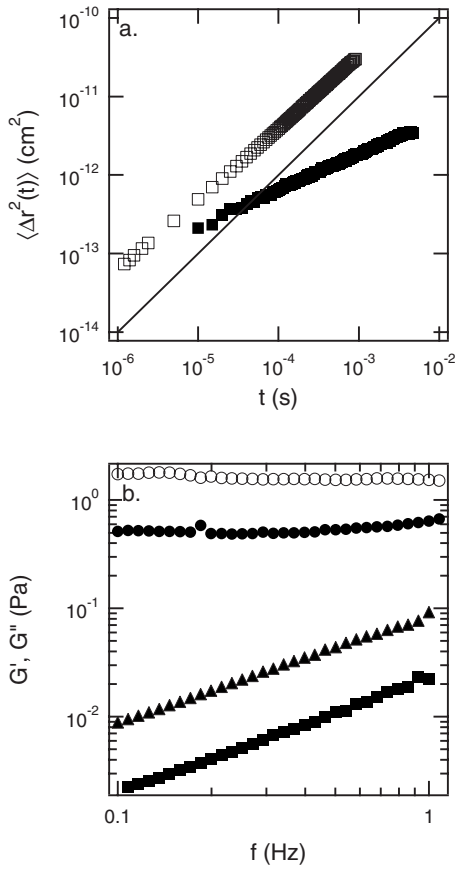

FIG. 3. (a) Mean-squared displacements of vesicles immediately after sample preparation measured by diffusing wave spectroscopy. Open squares: $\phi=0.3$ (vesicle only). Solid squares: $\phi=0.3$ and $C_P=2.0$ wt % for $R_g/a\approx 0.09$. The solid line has slope of 1 for comparison. (b) G' (open symbols) and G'' (solid symbols) immediately after sample preparation measured by frequency sweep experiments with $\sigma_0=0.01$ Pa. Circles: $\phi=0.3$ and $C_P=2.0$ wt % for $R_g/a\approx 0.09$. Triangles: $\phi=0.3$ (vesicle only). Squares: $C_P=2.0$ wt % (polymer only). For both control samples (polymer and vesicle only), only G'' is measurable.

respectively. We estimate the corresponding attractive interaction between particles using the Asakura-Oosawa (AO) theory [13] where $U(r)=-\Pi_P V_{overlap}(r)$ is the depletion potential between particles as a function of the center-to-center separation r. The polymer osmotic pressure Π_P is estimated based on the free volume at which the polymer coil can freely move [14]. The depletion volume $V_{overlap}$ is the volume of the overlapping depletion zones between two particles. Using the average of the polydisperse vesicle diameters, the gel line corresponds to $U\approx 15k_BT$ for $R_g/a\approx 0.09$ and $U\approx 5k_BT$ for $R_g/a\approx 0.27$ with the assumption that the vesicles are in contact.

Next, we examine the viscoelastic properties in the collapse regime to quantitatively verify the gel boundaries determined by visual inspection. The MSD $\langle \Delta r^2(t) \rangle$ of vesicles at $\phi=0.3$ for $R_g/a\approx 0.09$ measured by DWS is provided in Fig. 3(a). In the absence of polymer, the Brownian motion of vesicles is similar to pure self-diffusion, $\langle \Delta r^2(t) \rangle \sim t$. In contrast, the addition of polymer significantly increases the degree of subdiffusive dynamics, indicating the onset of arrested motion. Figure 3(b) shows corresponding storage and loss moduli measured by frequency sweep experiments with $\sigma_0=0.01$ Pa. Both control samples, including vesicles only ($\phi=0.3$) and polymer only ($C_P=2.0$ wt %), are nearly purely viscous solutions; consequently, we are able to measure only $G''(\omega)$ reliably. However, $G'(\omega)$ becomes larger than $G''(\omega)$ with 2.0 wt % of polymer. This reflects the formation of the gel network, corresponding to the onset of the elasticity in the vesicle network.

The height $h(t)$ of the vesicle-rich phase is captured as a function of time with a CCD camera under conditions where the collapse of vesicle gel is observed ($C_P \geqslant 0.3$ wt %). The results are shown in Figs. 4 and 5 for various ranges of vesicle volume fraction and polymer concentration ($\phi=0.05-0.3$ and $C_P=0.3-2.0$ wt %). The average of three measurements is shown, and no significant sample-to-sample variations are observed. In all cases, the collapse profiles are characterized by three distinct stages. Initially, the vesicle dispersion is stable and begins to rise slowly. Then, after a finite delay time, the gel collapses rapidly. Finally, it slowly compacts to a final equilibrium height h_f determined when $h(t)$ approaches a plateau. Overall, this behavior is typical of delayed sedimentation (delayed rising in our study) and is consistent with previous results for weakly aggregated colloidal gels [1,3–7]. However, we observe the unexpected dependence of polymer concentration on the height profile. As the polymer concentration increases, indicated by the arrow in Figs. 4 and 5, the initial delay time *decreases* and the vesicle network collapses faster. In contrast, typical gel collapse behavior shows significantly longer delay times, as the polymer concentration increases [6,7].

Delayed sedimentation has been observed for many weakly aggregated systems, but it is still poorly understood [1,3–7]. Kilfoil *et al.* [6] reported the scaling behavior of delayed sedimentation for silica spheres suspended in carboxymethylcellulose, suggesting a simplification of the wide variation in time scales for the onset of delayed sedimentation. Similarly, we normalize the height profile by $h'(t)=\frac{h(t)-h_f}{h_0-h_f}$ to eliminate the difference in final vesicle volume fractions for samples which reach an equilibrium height within 18 h. The normalized profiles $h'(t)$ are then scaled onto a single master curve with a time scaling factor α. As shown in Fig. 6(a), the vesicle system at $\phi=0.05$ provides a consistent scaling behavior with that reported by Kilfoil *et al.* [6]. Furthermore, from $h'(t)$, we determine the longest delay time τ_M at $h'(\tau_M)=0.1$ and the absolute delay time $\tau(C_P)=\tau_M/\alpha$ at fixed ϕ, respectively. Figure 6(b) shows calculated values of τ versus polymer concentration at $\phi=0.05$, which decrease as the polymer concentration increases. For instance, the vesicle dispersion with $C_P=0.3$ wt % are quiescent for nearly 2 h, while gels with $C_P=2.0$ wt % collapse almost immediately. Again, the dependence on τ with the polymer concentration is opposite to that of previous observations for delayed sedimentation under weak attractions [3–7]. We expected that stronger interparticle attractions as the polymer concentration increases would cause a slower evolution of the network collapse.

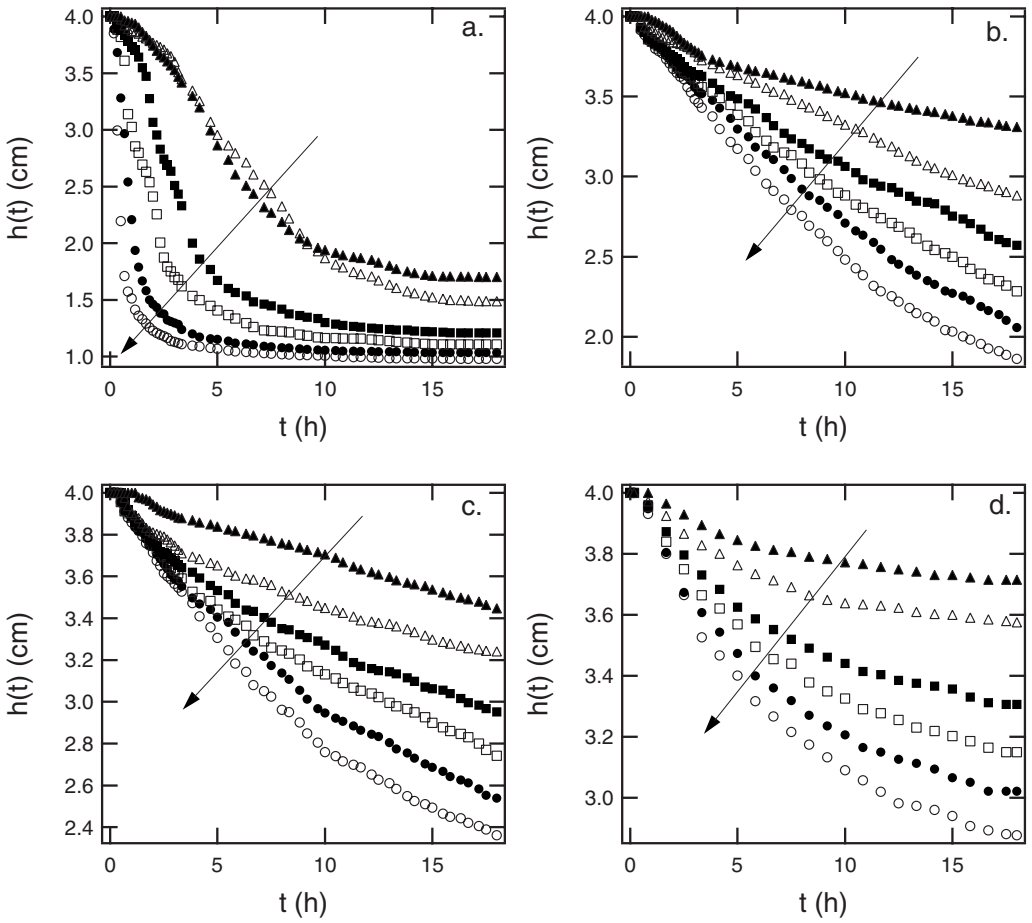

FIG. 4. Time evolution of the height as a function of polymer concentration for $R_g/a \approx 0.09$ at (a) $\phi=0.05$, (b) $\phi=0.15$, (c) $\phi=0.2$, and (d) $\phi=0.3$ for $C_P=0.3$ wt % (solid triangles), $C_P=0.6$ wt % (open triangles), $C_P=0.9$ wt % (solid squares), $C_P=1.2$ wt % (open squares), $C_P=1.6$ wt % (solid circles), and $C_P=2.0$ wt % (open circles). The arrow indicates the increase in polymer concentration from 0.3 to 2.0 wt%.

B. Microstructure

To understand anomalous collapse behavior, we next consider the evolution of the suspension microstructure with polymer concentration. The microstructure of vesicles dispersed in polyDADMAC solutions is imaged with fluorescence microscopy, as shown in Figs. 7 and 8 for $R_g/a \approx 0.09$ and 0.27, respectively. Figures 7(a) and 7(b) show the stable vesicle dispersion in the absence of polymer, indicating no change with time. In contrast, the microstructure begins to rearrange immediately after the polymer is added, as shown in Figs. 7(c), 7(e), 8(a), and 8(c). Importantly, at higher polymer concentrations, large pores are initially observable and their growth is significantly faster, as illustrated in Figs. 7(d), 7(f), 8(b), and 8(d). This change in microstructure likely facilitates the solvent backflow, which dominates the short-time behavior, leading to a faster collapse of the gel with increasing the polymer concentration. Under this possible mechanism, we can relate the sedimentation (rising in this study) of vesicle gels to the flow of a fluid through a porous medium [15].

We first obtain a characteristic length scale of the pores, by quantitatively analyzing the confocal images. For simplicity, we take two-dimensional confocal images perpendicular to the gravitational acceleration. All confocal images are taken at a fixed height approximately 150 μm from the bottom of the slide. Images are then thresholded to identify the individual pores. The two-dimensional number average pore length scale $\langle \xi \rangle_n$ is calculated in a pixel range greater than two vesicle diameters to reduce noise. Figure 9 shows the number average pore length scale $\langle \xi \rangle_n$ immediately after samples are prepared. We note that $\langle \xi \rangle_n$ increases nearly exponentially with polymer concentration and approaches a plateau at higher polymer concentrations, consistent with the trend observed for the sample height. Also, $\langle \xi \rangle_n$ decreases as the vesicle volume fraction increases. For instance, with the increase of ϕ from 0.05 to 0.3, $\langle \xi \rangle_n$ becomes smaller by a factor of 3 and 1.5 for the low- and high-MW polymers, respectively, as shown in Figs. 9(a) and 9(b), respectively. The characteristic pore sizes should be related to the fluid permeability in the network and, consequently, the collapse rate of the vesicles.

The permeability k is a key macroscopic property for describing viscous flow through a porous media and represents the proportionality constant between the average fluid velocity and applied pressure gradient [15]. In this study, we estimate the initial permeability k_0 based on Buscall and White's

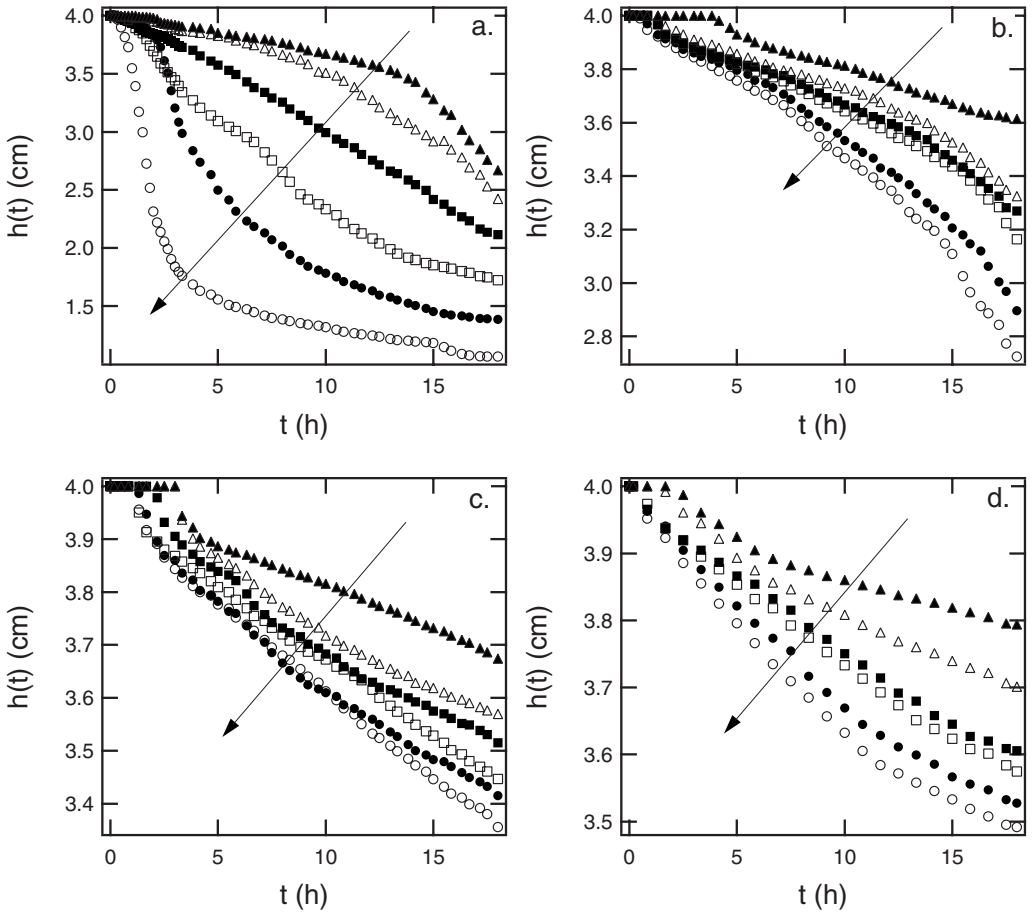

FIG. 5. Time evolution of the height as a function of polymer concentration for $R_g/a \approx 0.27$ at (a) $\phi=0.05$, (b) $\phi=0.15$, (c) $\phi=0.2$, and (d) $\phi=0.3$ for $C_P=0.3$ wt % (solid triangles), $C_P=0.6$ wt % (open triangles), $C_P=0.9$ wt % (solid squares), $C_P=1.2$ wt % (open squares), $C_P=1.6$ wt % (solid circles), and $C_P=2.0$ wt % (open circles). The arrow indicates the increase in polymer concentration from 0.3 to 2.0 wt%.

theory of the sedimentation of gels under a gravitational field [16]. Their model considers that the rate and extent of consolidation depends on a balance of three forces: the gravitational force, the viscous drag force associated with solvent flow in the sediment, and a particle or network stress developed as a result of direct particle-particle interactions. The initial rate of change of sediment height with time, $\frac{dh}{dt}|_0$, in a uniform gravitational field is given by

$$\left.\frac{dh}{dt}\right|_0 = -\frac{(1-\phi_0)u_0}{r(\phi_0)}\left[1-\frac{1}{B}\right], \quad B>1,$$

$$\left.\frac{dh}{dt}\right|_0 = 0, \quad B<1, \tag{1}$$

where $B=\frac{\Delta\rho g \phi_0 h_0}{P_Y(\phi_0)}$, $P_Y(\phi_0)$ is the compressive yield stress of the initial network, u_0 is the sedimentation rate of an isolated sphere $\left(u_0=\frac{2a^2\Delta\rho g}{9\eta_S}\right)$, ϕ_0 is the initial volume fraction of solids, $\Delta\rho$ is the difference in density between solid and liquid, g is the gravitational or centrifugal acceleration, and h_0 is the initial sediment height. The effect of hydrodynamic interactions can be accounted for by the drag coefficients and a dimensionless interaction parameter $r(\phi_0)$ with properties $r(\phi_0)\to\infty$ as $\phi_0\to 1$ and $r(\phi_0)\to 1$ as $\phi_0\to 0$. It can be estimated from the Carman-Kozeny permeability $k(\phi_0)=0.022a^2\frac{(1-\phi_0)^3}{\phi_0^2}$ or other semiempirical approaches [15] with $r(\phi_0)\sim a^2/k(\phi_0)$.

Equation (1) can be simplified further by assuming that the elastic properties of the gel contribute negligibly to the initial rising velocity. Many previous experimental studies have shown that the compressive yield and shear stresses increase with a power law dependence on the particle volume fraction [17–19]. At short times, the vesicle network is weakly, if at all, compressed and the dominant contribution to the collapse comes from the solvent backflow [7]. Under these circumstances, the compressive yield stress can be estimated by the shear modulus. This is a fairly reasonable assumption based on both DWS and rheology measurements, which both show that a very weak network has formed at short times [7]. Such small moduli result in large values of B, and the initial settling velocity is therefore initially independent of the compressive yield stress. Inverting Eq. (1), the initial permeability of the vesicle network can then be determined from the initial sedimentation velocity,

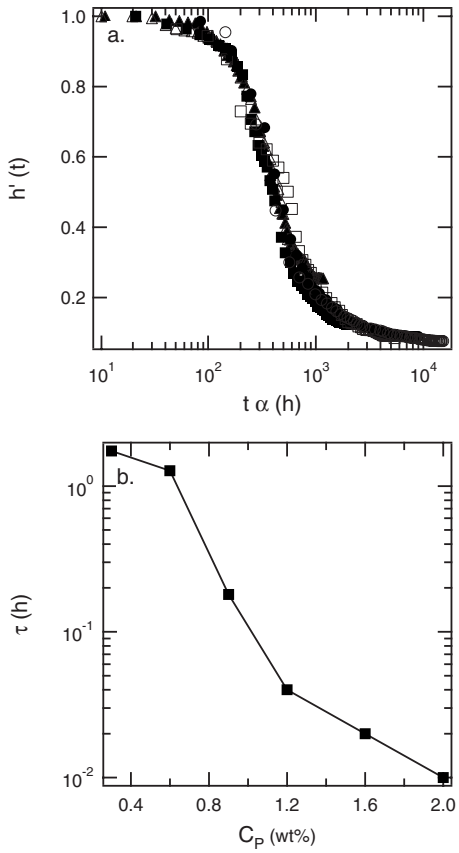

FIG. 6. (a) The normalized profiles $h'(t)$ exhibit a single master curve as a function of scaled time at $\phi=0.05$ and $R_g/a\approx 0.09$ for $C_P=0.3$ wt % (solid triangles), $C_P=0.6$ wt % (open triangles), $C_P=0.9$ wt % (solid squares), $C_P=1.2$ wt % (open squares), $C_P=1.6$ wt % (solid circles), and $C_P=2.0$ wt % (open circles). (b) The absolute delay time τ calculated from the normalized profiles $h'(t)$ as a function of polymer concentration for $\phi=0.05$ and $R_g/a\approx 0.09$.

$$k_0 \cong -\frac{a^2}{(1-\phi_0)u_0}\left.\frac{dh}{dt}\right|_0, \tag{2}$$

which is calculated from the slope of the height versus time data shown in Figs. 4 and 5 in the limit $t\to 0$.

We compare the resulting initial permeability k_0 with $\langle\xi\rangle_n^2$. Note that both k_0 and $\langle\xi\rangle_n^2$ exhibit the same dependence on vesicle and polymer concentrations; both increase with polymer concentration and decrease with vesicle volume fraction. Their remarkable similarity becomes further evident by the strong correlation demonstrated in Fig. 10. This enables us to account for the unexpected macroscopic collapse rate in terms of the microscopic structure of the networks. The increase in polymer concentration provides larger pore spaces corresponding to a more tenuous network. Then, the gel breakup is accelerated by faster solvent backflow in the network, leading to the collapse of the gel. Similarly, Manley *et al.* [5] reported a relationship between microstructure and permeability for fractal colloidal gels. They estimated k_0 as the free volume between ramified clusters. In that case, k_0

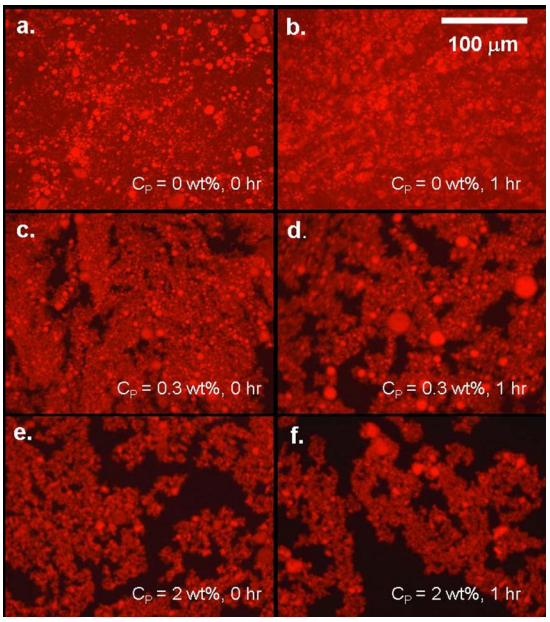

FIG. 7. (Color online) Short time-evolution in microstructure measured by fluorescence microscopy at $\phi=0.3$ and $R_g/a\approx 0.09$ immediately after sample preparation (a) $C_P=0$ wt %, (b) $C_P=0.3$ wt %, and (c) $C_P=2.0$ wt %; 1 h after sample preparation (d) $C_P=0$ wt %, (e) $C_P=0.3$ wt %, and (f) $C_P=2.0$ wt %. Vesicles are stained red.

$\sim R_c^2$, where R_c is the characteristic flow radius at the gel point.

What gives rise to these microstructures? At high ϕ and low $U_{\min}$ the attractive well of the interaction potential, similar to the system discussed here, phase separation occurs via spinodal decomposition. For instance, Carpineti and Giglio [20] find that the intensity distribution scale for the aggregation of dense colloidal solutions is in agreement with the scaling for spinodal decomposition. In contrast to fractal cluster aggregation at low ϕ and high $U_{\min}$, the space-spanning network is formed by the dynamic arrest within the

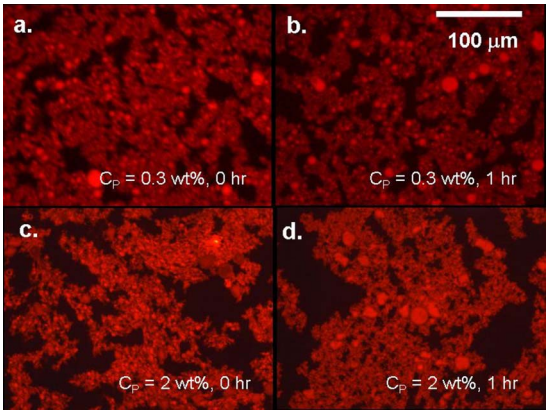

FIG. 8. (Color online) Short time-evolution in microstructure measured by fluorescence microscopy at $\phi=0.3$ and $R_g/a\approx 0.27$ immediately after sample preparation (a) $C_P=0.3$ wt % and (b) $C_P=2.0$ wt %; 1 h after sample preparation (c) $C_P=0.3$ wt % and (d) $C_P=2.0$ wt %. Vesicles are stained red.

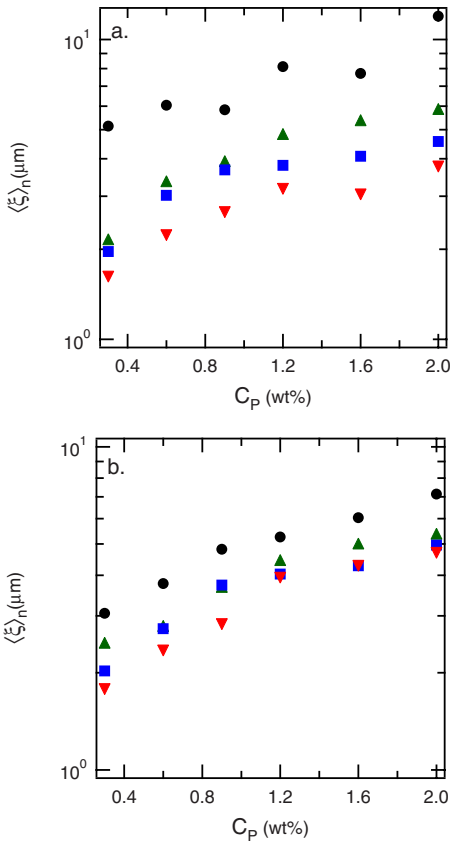

FIG. 9. (Color online) The characteristic pore length scale $\langle\xi\rangle_n$ obtained from the confocal microscopy as a function of polymer concentration at ϕ=0.05 (black circles), ϕ=0.15 (green upper triangles), ϕ=0.2 (blue squares), and ϕ=0.3 (red lower triangles) for (a) $R_g/a \approx 0.09$ and (b) $R_g/a \approx 0.27$.

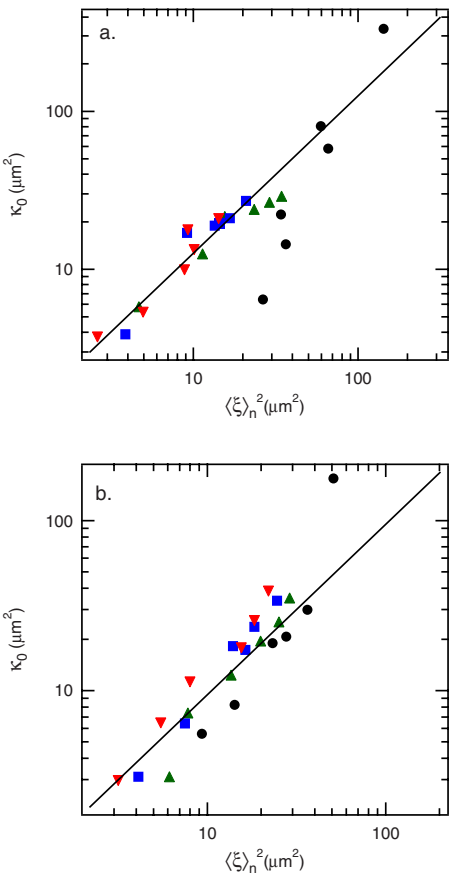

FIG. 10. (Color online) The characteristic pore area $\langle\xi\rangle_n^2$ shows the similar dependence on both polymer concentration and vesicle volume fraction to the initial permeability k_0: ϕ=0.05 (black circles), ϕ=0.15 (green upper triangles), ϕ=0.2 (blue squares), and ϕ=0.3 (red lower triangles) for (a) $R_g/a \approx 0.09$ and (b) $R_g/a \approx 0.27$. The line has a slope of 1 for comparison.

connected colloid-rich region during phase separation. Recently, Manley *et al.* [21] proposed that the arrest is driven by a *local* glass transition. At short times, our vesicle-polymer mixtures show more bicontinuous, locally arrested structures with increasing polymer concentration, as illustrated in Figs. 7 and 8, consistent with spinodal decomposition. Moreover, $\langle\xi\rangle_n$ increases rapidly with polymer concentration as shown in Fig. 9. This seems to be related to the initial rate of phase separation which is determined by the driving force for phase separation [22].

IV. CONCLUSIONS

We characterized the behavior of depletion-induced gels in vesicle-polymer mixtures. In the gel regime, the gel collapses faster and the delay time decreases with increasing polymer concentration. This unexpected collapse behavior is explained by the nearly one-to-one correlation between the porous microstructure, determined by microscopy, and the solvent permeability from the initial rising velocity. In contrast, previous studies of gel collapse using monodisperse particles have shown that the velocity and delay time increase with increasing attractive interactions. The microscopic mechanisms responsible for this intriguing difference remain an open question. Vesicles possibly experience different interparticle attractions that strongly depend on their dimensions. The softness of the repulsion between vesicles may also enable rearrangements and a later onset of arrest during phase separation.

ACKNOWLEDGMENTS

We thank David Weitz, Alberto Fernandez-Nieves, William Russel, and Tom Kodger for helpful discussions. This research was supported by The Procter & Gamble Company, NSF (Grant No. CBET-0238689), and the DuPont Young Investigator Program.

[1] W. C. K. Poon, L. Starrs, S. P. Meeker, A. Moussaid, R. M. L. Evans, P. N. Pusey, and M. M. Robins, Faraday Discuss. **112**, 143 (1999).
[2] N. A. M. Verhaegh, D. Asnaghi, H. N. W. Lekkerkerker, M. Giglio, and L. Cipeletti, Physica A **242**, 104 (1997).
[3] L. Starrs, W. C. K. Poon, D. J. Hibberd, and M. M. Robins, J. Phys.: Condens. Matter **14**, 2485 (2002).
[4] R. M. L Evans and L. Starrs, J. Phys.: Condens. Matter **14**, 2507 (2002).
[5] S. Manley, J. M. Skotheim, L. Mahadevan, and D. A. Weitz, Phys. Rev. Lett. **94**, 218302 (2005).
[6] M. L. Kilfoil, E. E. Pashkovski, J. A. Masters, and D. A. Weitz, Philos. Trans. R. Soc. London, Ser. A **361**, 753 (2003).
[7] V. Gopalakrishnan, K. S. Schweizer, and C. F. Zukoski, J. Phys.: Condens. Matter **18**, 11531 (2006).
[8] D. D. Lasic, *Liposomes: From Physics to Application* (Elsevier, Amsterdam, 1993).
[9] M. J. Ostro, *Liposomes: From Biophysics to Therapy* (Dekker, New York, 1987).
[10] V. P. Torchilin and V. Weissig, *Liposomes: A Practical Approach* (Oxford University Press, Oxford, 2003).
[11] M. L. Lynch, T. Kodger, and M. R. Weaver, J. Colloid Interface Sci. **296**, 599 (2006).
[12] D. J. Pine, D. A. Weitz, J. X. Zhu, and E. Herbolzheimer, J. Phys. (Paris) **51**, 2101 (1990).
[13] S. Asakura and F. Oosawa, J. Polym. Sci. **33**, 183 (1958).
[14] S. M. Ilett, A. Orrock, W. C. K. Poon, and P. N. Pusey, Phys. Rev. E **51**, 1344 (1995).
[15] J. Happel and H. Brenner, *Low Reynolds Number Hydrodynamics* (Prentice-Hall, Englewood Cliffs, NJ, 1965).
[16] R. Buscall and L. R. White, J. Chem. Soc., Faraday Trans. 1 **83**, 873 (1987).
[17] G. M. Channell and C. F. Zukoski, AIChE J. **43**, 1700 (1997).
[18] C. J. Rueb and C. F. Zukoski, J. Rheol. **41**, 197 (1997).
[19] R. Buscall, I. J. McGowan, P. D. A. Mills, R. F. Stewart, D. Sutton, L. R. White, and G. E. Yates, J. Non-Newtonian Fluid Mech. **24**, 183 (1987).
[20] M. Carpineti and M. Giglio, Phys. Rev. Lett. **68**, 3327 (1992).
[21] S. Manley, H. M. Wyss, K. Miyazaki, J. C. Conrad, V. Trappe, L. J. Kaufman, D. R. Reichman, and D. A. Weitz, Phys. Rev. Lett. **95**, 238302 (2005).
[22] R. G. Larson, *The Structure and Rheology of Complex Fluids* (Oxford University Press, Oxford, 1999).